Published in final edited form as:
Int J Hyperthermia. 2013 ; 29(2): 106–120. doi:10.3109/02656736.2013.764023.

Method to reduce non-specific tissue heating of small animals in solenoid coils

ANANDA KUMAR[1,★], **ANILCHANDRA ATTALURI**[2,★], **RAJIV MALLIPUDI**[2], **CHRISTINE CORNEJO**[2], **DAVID BORDELON**[2], **MICHAEL ARMOUR**[2], **KATHERINE MORUA**[3], **THEODORE L. DEWEESE**[2], and **ROBERT IVKOV**[2]

[1]Lambda Z Technologies, Baltimore

[2]Department of Radiation Oncology and Molecular Radiation Sciences, Johns Hopkins University School of Medicine, Baltimore

[3]Department of Biomedical Engineering, Johns Hopkins University, Baltimore, Maryland, USA

Abstract

Purpose—Solenoid coils that generate time-varying or alternating magnetic fields (AMFs) are used in biomedical devices for research, imaging and therapy. Interactions of AMF and tissue produce eddy currents that deposit power within tissue, thus limiting effectiveness and safety. We aim to develop methods that minimise excess heating of mice exposed to AMFs for cancer therapy experiments.

Materials and methods—Numerical and experimental data were obtained to characterise thermal management properties of water using a continuous, custom water jacket in a four-turn simple solenoid. Theoretical data were obtained with method-of-moments (MoM) numerical field calculations and finite element method (FEM) thermal simulations. Experimental data were obtained from gel phantoms and mice exposed to AMFs having amplitude >50kA/m and frequency of 160 kHz.

Results—Water has a high specific heat and thermal conductivity, is diamagnetic, polar, and nearly transparent to magnetic fields. We report at least a two-fold reduction of temperature increase from gel phantom and animal models when a continuous layer of circulating water was placed between the sample and solenoid, compared with no water. Thermal simulations indicate the superior efficiency in thermal management by the developed continuous single chamber cooling system over a double chamber non-continuous system. Further reductions of heating were obtained by regulating water temperature and flow for active cooling.

Correspondence: Robert Ivkov, David H. Koch Cancer Research Building, Room 442, Department of Radiation Oncology and Molecular Radiation Sciences, Johns Hopkins University School of Medicine, 1550 Orleans Street, Baltimore, MD 21231, USA. Tel: 443-287-7282. Fax: 410-502-2821. rivkovl@jhmi.edu.

★Ananda Kumar (EM simulations, experimental design, and manuscript preparation) and Anilchandra Attaluri (thermal simulations, data analysis, and manuscript preparation) contributed equally to the paper.

Declaration of interest: This work was funded by an award from Safeway Foundation and the Prostate Cancer Foundation. Ananda Kumar is an employee of Lambda Z Technologies, an EM design and engineering company. All other authors report no conflicts of interest. The authors alone are responsible for the content and writing of the paper.

Conclusions—These results demonstrate the potential value of a contiguous layer of circulating water to permit sustained exposure to high intensity alternating magnetic fields at this frequency for research using small animal models exposed to AMFs.

Keywords

magnetic induction; solenoid coil; hyperthermia; thermal therapy; water

Introduction

Solenoid coils are used in biology and medicine for research, imaging and therapy as devices that generate radiofrequency (RF) alternating magnetic fields (AMFs) [1–7]. Magnetic nanoparticle hyperthermia for cancer therapy is an application of solenoids that may benefit with high intensity AMF because magnetic nanoparticle heating depends upon both AMF frequency and amplitude [6, 8, 9]. Generally, the goal of such research is to develop nanoparticle and solenoid combinations that produce a maximum particle-associated heating rate, or loss power for a given flux (peak-to-peak) magnetic field, or *B*-field. For many magnetic materials, the loss power increases both with increasing AMF frequency and with amplitude, thus encouraging development of devices that generate high amplitude fields for a given frequency [9, 10]. Indeed, some nanoparticle formulations produce insignificant heating unless exposed to high amplitude fields at a given frequency [9, 10], thereby motivating combinations with high frequency or high amplitude devices in research for magnetic nanoparticle hyperthermia. While both device and nanoparticle research have accelerated in recent years, there is relatively little systematic study describing thermal management for bodies exposed to AMFs.

It is generally accepted that non-specific heating from exposure to the magnetic component (*B*-field) of low frequency electromagnetic (EM) fields occurs primarily via tissue coupling through magnetic induction by producing an electric field within the tissue, or a charge imbalance and associated eddy currents. Tissue heating from AMFs strongly depends upon the intensity and frequency of the field, and the dielectric permittivity and electrical conductivity of tissue(s) [3, 11–19]. The extent of non-specific power absorption that leads to heating thus depends on the AMF amplitude (*H*), frequency (*f*), and varies along the radial distance (*r*) of the sample [20, 21].

$$P_{Non-specific} \propto \sigma_t (\pi \times \mu_0 \times r \times f \times H)^2 \quad (1)$$

where, σ_t is electrical conductivity of the cylinder (idealised tissue) and μ_0 is the permeability of vacuum. Results obtained by Atkinson et al. [20] indicate that maximum tolerable exposure to fields produced by a 30-cm long single-turn induction coil can be approximated by the product $f \times H < 4.85 \times 10^8$ A/(m × s) for a phantom of a human torso having $r = 0.15$ m. Using this relationship, the allowable power deposition as a function of *H* and *f* with *r* fixed at 0.15 m can be estimated and is shown in Figure 1A; and deposition as a function of *H* and *r* at a fixed frequency of 160 kHz is shown in Figure 1B. It is worth emphasising that this estimate of maximum tolerable power deposition considers human

torso exposure, and can likely be exceeded for localised exposure of smaller regions such as head, neck, or limbs. The latter have not been adequately explored.

Heat generated in tissues exposed to alternating *B*-fields arises from charge imbalances created in tissues, and depends upon the dielectric permittivity and electrical conductivity of tissue(s) [11–19]. For medical devices it thus becomes critical to develop technology that provides magnetic fields having the desired properties at the region of interest while simultaneously minimising the undesired effects of interactions between the patient and the energy source. The time-rate of change of temperature (*dT*/*dt*) within a non-perfused body arising from EM-induced specific absorption rate (SAR) can be written as in Equation 2.

$$\frac{\mathrm{d}T}{\mathrm{d}t}=\frac{1}{\rho c}(\nabla\cdot(k\nabla T)+(\mathrm{SAR}\times\rho)) \quad (2)$$

where ρ is the mass density (kg/m^3), c the heat capacity (J/kg°C), and k is the thermal conductivity of tissue. In biological tissue having local and finite conductivity σ (S/m), the SAR is given by [13, 15] Equation 3.

$$\mathrm{SAR}=\frac{\sigma\left|\vec{E}_T\right|^2}{\rho}. \quad (3)$$

Here $\vec{E}_T$ refers to total induced electric field in the tissue, arising consequent to exposure of the body to time-varying *B*-field.

Heat is a potent anticancer and radiation-sensitising agent that causes profound biological changes in cells [15, 22–27]. For cancer therapy it has been suggested that AMF can be combined with magnetic nanoparticles that are locally concentrated in cancer tissue to selectively heat the cancer [8, 28–31]. For a specific AMF frequency, the heat generated by the nanoparticles generally depends upon the magnitude or intensity of the AMF [8–10]. Thus therapeutic efficacy of such magnetic nanoparticle hyperthermia (MNH) can be enhanced with high intensity fields applied to those regions of tissue that contain tumours bearing high concentrations of magnetic nanoparticles [31]. Nanoparticles capable of generating therapeutic heating at low AMF amplitudes are certainly advantageous; however, such formulations are not yet readily available. Furthermore, even low amplitude fields can deposit power to tissues when the volume of tissue exposed is large, and long exposure times can lead to unsafe overheating. For clinically relevant applications with MNH, exposure to AMF field with useful amplitude (*H*), frequency (*f*), and duration can result in tissue heating, creating a need to develop techniques that minimise non-specific heating or resulting temperature elevations *in vivo*.

Early stage MNH research is generally performed on small rodents, i.e. mice and rats [32, 33]. During MNH animals are anaesthetised, whereupon the animals become hypothermic because normal thermoregulatory controls are temporarily compromised [16, 17, 33]. Heat loss occurs through respiration and body surface cooling if ambient temperatures are significantly lower than the physiological norm. These effects are typically countered by

covering the animal to minimise heat loss and the animal is actively warmed on a heating pad. Care must be exercised, however to avoid lethal overheating or hyperthermia, to maintain body temperature of the animal below 40° C. For effective MNH, animals may be subjected to an AMF that can cause significant temperature increases [32, 33]. Warming pads and coverings may therefore be unsuitable because supplementary heating may interfere with the AMF [33].

Using numerical simulations, Trakic et al. [32] have shown a possible temperature elevation range of 0–8°C based on the spatial relationship of a mouse position with respect to a high intensity and low frequency AMF localised to a portion of the mouse and not the whole body. The model, however did not consider compromised thermal regulation in anaesthetised animals. Therefore, in regional or whole-body MNH experiments, hypo- and hyperthermic states can coexist in the same animal at different locations. In other words, a substantial temperature gradient can exist within the animal, causing significant stress, potentially affecting survival, and complicating data collection and analysis. Previous data obtained by exposing mice to high flux density inhomogeneous fields [33] demonstrates the importance of maintaining rectal temperature below 41°C during MNH. If MNH is performed without regulating body temperature, the animal is subjected to the substantial temperature gradients and thermal fluctuations throughout the body. This compromises the effectiveness of the therapy and may lead to death [6, 16, 17, 20, 30, 31, 33]. For MNH, magnetic resonance imaging (MRI), and other EM-based medical equipment, it thus becomes critical to develop thermal management systems that minimise these thermal gradients and compensate for both excessive cooling (loss of thermoregulatory control) and heating (interactions with EM fields).

We developed a water jacket to maintain the body temperature of the animal without interfering with the AMFs that are desired for MNH. In this study we performed numerical field simulations, thermal simulations, and initial feasibility experiments with tissue equivalent gel phantoms, and then on nude mice. Strain and gender of mice used in this study were selected because they are consistent with those used for nanoparticle-based cancer therapy experiments. We report results demonstrating that the designed water jacket was able to regulate and maintain mouse body temperatures well within tolerable limits, even with extremely high intensity fields (>80kA/m) having a frequency of 160 kHz.

Materials and methods

Alternating magnetic field system

The AMF system comprises three main components: (1) the power source, (2) an external impedance matching (capacitance) network, and (3) the load. The load comprises an inductor, or solenoid coil. The power source, matching network, and inductor were cooled with an industrial (80-kW-rated) closed-loop circulating water/water cooling system comprising a 200-L reservoir of distilled water that is pumped through the RF system at a flow rate of 170L/min and pressure 6 atm.

The power supply was an 80-kW induction heating system manufactured by PPECO (Watsonville, CA, USA) that provides an alternating current to a resonant circuit with

variable frequency between 135 kHz and 440 kHz. The power supply (source) impedance was adjusted to match the coil and capacitance network by adjusting its internal inductance and capacitance. Matchbox and inductor electrical properties were measured using an LCR meter (QuadTec, Newton, MA, USA).

The external capacitance network (AMF Life Systems, Auburn Hills, MI) was adjusted for stable oscillation at 160 ± 1 kHz with a total capacitance of 1.33 μF with five 0.2 μF and one 0.33 μF capacitors, each rated to provide up to 400 A at maximum of 1 kV. A circuit diagram is provided in Figure 2A.

Inductor or solenoid coil

A four-turn solenoid with inner diameter of 45.5 mm, outer diameter of 57.5 mm, and a length of 32 mm was constructed from dehydrated annealed soft copper refrigerator tubing having 6.4 mm outer diameter (OD). Schematics of the circuit diagram and coil are shown in Figure 2 A and B, respectively. To maintain the high electrical conductivity of the pre-annealed copper tubing, the coil was formed with a minimum of cold working. The coil was connected to the matching network with 10-mm diameter Swagelok® brass tubing connectors to copper plates affixed to solid copper capacitance busses (AMF Life Systems). Measurements of the AMF amplitude were taken in the centre of the coil with a magnetic field probe (AMF Life Systems) that measures magnetic flux lines in two orthogonal dimensions. The probe and methods used to map fields have been previously described [9, 34]. The field amplitude was measured in the coil centre before each set of trials. The measured amplitude in this point is reported as the experimental amplitude.

Temperature measurements

Temperatures were measured with three RF-resistant fibre-optic temperature probes (FISO, Quebec, Canada) in gel phantoms, two at the phantom periphery at opposing positions, and one in the centre. For mouse measurements, four probes were used: two were placed subcutaneously in the left and right thoracic regions, one in the rectum, and the fourth was fixed to the skin (surface) of the abdomen because this portion of the mouse was in contact with the surface of the mouse chamber and water jacket (see below). Subcutaneous probe placement was selected because SAR equations, thermal simulations (see below), and previously published data suggest that the power deposition primarily occurs at the periphery of the body (i.e. max r), [7, 13, 16, 20, 21, 32, 33]. Thus, implanting temperature probes into deep tissues (i.e. intramuscular), was expected to provide a less precise measure of immediate temperature changes resulting from EM-tissue interactions. Temperatures were recorded at 1-s intervals, beginning after samples, i.e. phantoms or mice, were in place for about 30 s and before AMF exposure. For mouse experiments, temperatures were measured from sham controls (no AMF power) for each condition. These data were subtracted from experimental temperatures to correct for heating from the water jacket which was maintained at 35°C.

Water jacket and mouse chamber

The water jacket was constructed from concentric poly-acrylic tubing (inner diameter = 38 mm and wall thickness ~3.2 mm) that was filled with distilled water. To make the water

cage device, two holes were drilled into the tube at opposite ends. Acrylic hose adapters (6 mm) were screwed into the holes with Teflon tape as a sealant. The coil and prototype water jacket are shown in Figure 3.

The gel phantom chamber was constructed from standard polypropylene 50 mL conical centrifuge tube into which the gels were poured, having an inner diameter of 30 mm. The 50-mL conical tube was suspended in the acrylic tube by two rubber O-rings at both ends of the tube. Adhesive silica caulk was applied to ensure a water-tight seal at the ends of the acrylic tubing. No water was used in the acrylic tubing device for tests of the no-water condition (condition I).

For tests with both gel phantom tube and water jacket, distilled water from a separate closed-loop bench-top circulating bath (Hoefer Scientific Instruments, San Francisco, CA) capable of circulating water at 4L/min was used. For some measurements the temperature of the water was adjusted with the circulating bath operating until a steady temperature (±0.5°C within target) was achieved. Once the desired temperature was achieved, the pump was turned off (condition II). For the thermal management of the animal i.e., water circulation in the jacket (condition III), the water temperature was set to 35 ± 0.5°C and the circulating bath operated continuously during the 20-min AMF exposure.

Once built, we characterised the thermal properties of the jacket and coil at several power settings to determine power absorption by water in the jacket. The temperature of the coil and jacket were monitored for 20-min AMF power applications with amplitude settings of ~16, 32, 48, 64, 80, and 94kA/m (data not shown). The temperature of the water in the jacket was set to between ~0.5° and 1.0°C of the anticipated steady-state coil temperature for each power setting. The latter was determined by separate measurements. Temperatures were recorded with two fibre-optic temperature probes: one was taped to the outer coil surface near its centre, and the other was attached to the inside surface of the jacket with the probe tip just outside the coil. The final jacket temperature, after 20 min, was then subtracted from the coil steady-state temperature. A series of tests were conducted with no water in the jacket to characterise heating or power absorption by the materials comprising the mouse chamber (data not shown). The mouse chamber temperature never rose above the coil temperature for any tested power condition when the chamber contained no water. The data suggest that the chamber or materials do not absorb power.

Numerical simulations

Numerical calculations performed in this study were based on the Method of Moments (MoM) volume equivalence principle (VEP) [35, 36] using FEKO (EM Software and Systems, Stellenbosch, South Africa) for EM calculations, and FEM thermal simulations were done with COMSOL Multiphysics (COMSOL, Burlington, MA).

Magnetic field simulations

The modelled solenoid coil is shown in Figure 2B. The analytical expression for inductance of the AMF solenoid is shown in Equation 4.

$$L_{AMF}=L_S+2L_1-2M_1 \quad (4)$$

where L_s is the solenoid inductance, L_1 is the inductance of the lead wire extension from the tuning (match) box and M_1 is the mutual inductance between the parallel lead wire extension. The solenoid inductance is given by Equation 5 [37].

$$L_S=\frac{\mu N^2 A}{l} \quad (5)$$

where μ is the permeability of free space, N, number of turns, A, cross-sectional area of coil, and l is the length of coil. The self-inductance of the lead wire extension L_1 is given by Equation 6 [37].

$$L_1=0.002l_{lead}\left(\ln\frac{2l_{lead}}{r}-1\right) \quad (6)$$

here l_{lead} refers to the length of the lead wire extension and r is the radius of the wire. The mutual inductance M_1 between a parallel lead wire of length l_{lead} separation distance d is given by Equation 7 [37].

$$M_1=0.002l_{lead}\left[\ln\left(\frac{l_{lead}}{d}+\sqrt{1+\frac{l_{lead}^2}{d^2}}\right)-\sqrt{1+\frac{l_{lead}^2}{d^2}}+\frac{d}{l_{lead}}\right] \quad (7)$$

For MoM simulation the solenoid was tuned to resonate at 160 kHz with ~1.2 μF capacitance in the tuning box. The experimental capacitance was adjusted to 1.3 μF.

Thermal simulations

Heat transfer analysis was performed on a 3D cylindrical domain with radius of 1.9 cm and length of 6 cm. Transient Pennes bioheat equation based on energy balance is used to model the tissue temperature (T_t) within the cylindrical domain.

$$\rho_t C_{t-p}\frac{\partial T_t}{\partial t}=k_t\nabla^2 T_t+\omega\rho_b C_{b_p}(T_b-T_t)+q_m+Q \quad (8)$$

Subscripts t and b refer to tissue and blood, respectively; ω is local blood perfusion rate, T_t is the tissue temperature, k_t is tissue thermal conductivity, ρ is tissue density, c_p is specific heat, T_b is arterial temperature, q_m is volumetric heat generation rate due to metabolism and Q is the volumetric heat generation rate. Volumetric heat generation rate is modelled based on Equation 1. The effect of rate of metabolic heat generated is neglected. The parameters used for simulation are listed in Table I. In the present study the mice are anaesthetised, which minimises their thermal regulation capabilities (16, 17, 33). Hence, a constant blood perfusion can be assumed. Three different cases are modelled for this study.

No external cooling—All surfaces are subjected to convective cooling at room air temperature (h = 10 W/(m^{2}K) and T_{air}= 20°C). Simulation setup of the no external cooling is similar to condition I in the mouse experiments (see below).

Dual chamber discontinuous cooling—The two radial surfaces are exposed to air at room temperature. Two opposite sides of the four surfaces along the length of the cylinder are subjected to external cooling with flowing water. The water temperature and flow rate are set to 35 °C or 27 °C and 4L/min respectively.

Single chamber continuous cooling—The two radial surfaces are exposed to air at room temperature. All surfaces along the length of the cylinder are subjected to external cooling with flowing water. The water temperature and flow rate are set to 35°C and 4L/min respectively. The single chamber continuous cooling simulation set-up is similar to condition III in the animal experiments, but here we assume perfect contact of the water cooled surfaces with the simulation domain which is not the case in mouse experiments (see below).

Gel phantoms

The thermal effect was experimentally measured with 1% w/w agar gel phantoms (Sigma Aldrich, Saint Louis, MO) containing 0.035 M NaCl prepared in the 50-mL centrifuge tubes following established methods for mimicking physiological electrical conductivity of muscle tissue at 200 kHz [38]. Three temperature probes were used to monitor phantom temperatures. One temperature probe was placed in the radial centre of the phantom (core) whereas the other two were placed 5 mm from the opposing side walls of 50-mL tubing at the centre of the solenoid.

Temperature measurements were performed in the phantom without water (condition I) and with water (condition II) in the jacket, and with water circulating in the jacket (condition III). To test active thermal regulation, water was flowed through the device at 20°C. Water entered the tube from the bottom and exited through the upper connector to ensure mixing. Air bubbles were removed to enhance the flow of water and to ensure the continuity of the water layer.

Mice

Six male BALB/c nu/nu mice (Harlan Labs, Indianapolis, IN) were used in this study. All were 5–8 weeks old and weighed 21–26 g (mean 22 ± 2g) prior to treatment. They were maintained according to Johns Hopkins University School of Medicine guidelines on a normal diet, *ad libitum.* All methods described were approved by the Institutional Animal Care and Use Committee.

Each mouse was anaesthetised by intraperitoneal injection of a ketamine (100 mg/kg body mass)/xylazine (10 mg/kg) solution in 0.9% saline. The solution was filtered through a 0.2 μm filter. Sufficient anaesthesia was determined by the lack of a reflexive response when a hind paw was lightly compressed.

After each mouse was anaesthetised four fibre-optic temperature probes were positioned: one in the rectum, two subcutaneous (s.c.) in the dorsal thorax and contralateral thorax to mimic the probe testing locations done in the agar (top, core, bottom). The fourth and final probe was taped to the skin on the ventral surface, level with the s.c. probes. The s.c. probes were inserted with the aid of a 19-gauge 1.5-inch hypodermic needle, and once positioned the mouse was placed into a holder fashioned from a 50-mL centrifuge tube.

Each mouse was placed in the chamber and positioned so that the s.c. and ventral probes were aligned with the centre of the solenoid to ensure maximum exposure to high amplitude field. Experiments at conditions I (no water) and II (with water) were performed without active temperature regulation in the mouse chamber. For condition III the temperature-controlled water in the jacket was maintained at 35°C by circulation through the chamber, thus actively regulating the temperature in the treatment chamber. Temperatures for each experiment were recorded with FISO software for 20 min of AMF exposure at 86 ± 3 kA/m (ppk) at 160.1 ± 0.5 kHz (as with gel phantoms) and for a brief ‘cool-down’ period after AMF shutdown.

Results

The principal objective of this study was to develop a thermal management device and methods that minimise excess heating of small animals that are exposed to high amplitude radiofrequency alternating magnetic fields. To accomplish this we built a single chamber continuous water flow cooling device. Presented here are numerical results that compare the relative performance of this thermal regulation device with a two-chamber device previously described [39].

Magnetic field

As a first step, we compared the numerically predicted coil inductance with inductance values obtained from measurement and analytic calculations. The simulation results agreed to within 3% of measured and calculated inductance (Table II), confirming the general validity of the MoM model. The inductance was then used to calculate the magnetic field values for a range of applied voltages using both simulation and analytical expressions. The results of these calculations and their comparison with experimental results are listed in Table III. The agreement between experimental and calculated values was within 7% of calculated values. This agreement is adequate given the uncertainties possible with spatial positioning of a probe within a simple solenoid having significant field inhomogeneities [34].

Magnetic fields inside the solenoid with and without water were calculated, and the resulting field maps are shown in Figures 4A and B. Figures 4C and D show the magnetic field profile along the z direction in the middle of the coil across the x–z plane within the AMF coil, without water and with water, respectively for 8 kW input power to the coil. This simulated power approximately translates to a field intensity of 80 kA/m in the coil centre (Table IV). The simulated field maps (Figure 4) and data in Table IV demonstrate that the magnetic field in the coil is unaffected by the presence of water. Further, no measurable differences of field amplitudes were observed with water circulating through the water

jacket in the solenoid. The experimentally measured values are reported in Table IV. The two groups showed no statistically significant differences when tested using single-factor ANOVA.

Thermal simulation

Temperature profiles at the end of 20 min of exposure to AMF (84 kA/m and 160 kHz) from FEM heat transfer simulations are shown in Figure 5A–D. With no external cooling, simulated temperatures reach up to ~42°C (Figure 5A). Dual chamber discontinuous cooling with water temperature at 35°C reduced the averaged domain temperature but failed to reduce the overall maximum domain temperature below ~40°C (Figure 5B). When the water temperature was reduced to 27°C from 35°C the temperature of the core is maintained within the physiological range but it is achieved by creating a significant thermal gradient in hypothermic ranges (~27–37°C) across the domain (Figure 5C). The best results among the test cases are observed for the single chamber continuous cooling with water temperature at 35°C as expected. The core temperature is always in the physiological range and the temperature gradients across the domain are minimised (35–38°C) for the single chamber continuous cooling case (Figures 5D and E). The results from no external cooling and single chamber continuous cooling cases are comparable to the spatial temperature elevations measured at the end of 20 min AMF exposure in mice for conditions I and III respectively.

Gel phantom data

For gel phantom measurements, the AMF system was tuned to maintain a measured field intensity of 86 ± 3 kA/m (ppk) at 160.1 ± 0.5 kHz for continuous operation (100% duty cycle) for 20 min. Measured temperature changes are reported in Table V, i.e. $\Delta T = T(t) - T(t = 0)$, for each condition. Because the solenoid has an axisymmetric design and field, the eddy current production and thus temperature change of the opposing radial edges of the gel in the centre of the coil were assumed to be equal. Experimental measurements confirm this to within ± 0.5°C, thus the mean of the two radial values is reported in Table V. In condition III the net temperature change at the centre of the gel is reduced almost 10-fold when compared with condition I. The circulating water in the jacket has caused an apparent redistribution of the temperature profile within the sample. In condition I, the edge or ‘skin’ temperature is higher than at the core; however, this difference reverses in condition III and the gel core shows a higher temperature than the ‘skin’, although both are significantly lower than in condition I.

In addition to modulating net temperature change, active cooling apparently modifies the initial rate of rise of temperature in the gels. A two-fold reduction of initial temperature rise is shown in Figure 6 for gel phantom experiments from condition II (without any effective thermal management, just in the presence of non-circulating water) to condition I. Condition III (circulating water) with constant flow rate and controlled temperature displays a further reduction of the initial rate of temperature rise. Similar trends were observed in the FEM simulations and animal experiments.

Mouse data

With no applied AMF, mice experience a net temperature decrease at the end of 20 min when placed within the solenoid. Net temperature decreases in the AMF sham cohort of mice (i.e. no AMF exposure) for conditions I and II were 3–5°C and 1–2°C, respectively at various locations of the body. For condition III, however, there was a corresponding increase of net temperature <1°C for sham control. The results for the sham controls are provided in Table VI and shown in Figure 7A. Without a thermally regulated water jacket, mice are exposed to the hypothermic conditions of coolant flowing through the inductor (~20°C), losing heat through conduction. Conversely, contact with actively regulated water near physiological temperature (35°C) provides a thermally stabilising environment to counteract the loss of thermoregulatory control. The net temperature increase in mice with respect to sham (i.e. difference between sham and treatment groups) at the end of 20 min of AMF treatment are shown in Table VI and Figure 7B. Net temperature change range that was measured at various locations of the body for conditions I, II, and III were 8–12°C, 2–6°C and <2°C respectively. A two-fold decrease in temperature change (increase) was observed from conditions I to II (Table VI). When compared to condition I, condition III demonstrates a significantly reduced temperature increase. A six-fold drop in the temperature rise was observed from condition I. This suggests that convective heat dissipation was least effective to manage non-specific tissue heating and that actively flowing thermally regulated water through the mouse chamber was most beneficial. Figures 8A and B show mean s.c. and rectal temperatures, respectively, for mice under all conditions, with sham data subtracted, summarising the results.

Discussion

Magnetic nanoparticle hyperthermia is one of many applications in biology and medicine that expose tissues or bodies to time-varying EM fields. Tissue interactions with EM fields deposit power, creating thermal gradients and causing stress. The amount of heat deposited in a region of tissue is proportional to the product of frequency and field amplitude, both exponent two. Similarly, magnetic materials generate heat when exposed to time-varying magnetic fields, but by different mechanism than in tissues. While the dependence of magnetic heating on AMF parameters differs from that of tissues, for magnetic materials the loss power increases both with increasing AMF frequency and with amplitude, thus encouraging exploratory work to develop systems that generate AMFs optimal for MNH. Limiting the inductor design specifications, however, are considerations of safety vis à vis non-specific tissue heating. In the current work we systematically explore the benefits of active thermal regulation with water for research devices designed for small animals used in exploratory research for MNH. Exposure to high amplitude fields was the test condition to demonstrate the potential benefit of such regulation because this represents a challenging case. Further, currently available nanoparticle formulations typically exhibit therapeutic loss power only at high amplitudes (near magnetisation saturation) [9, 10].

In the present work, temperature measurements of both phantom gel and animals showed significantly moderated averages in the centre or core for both conditions II and III (with water) compared to condition I (no water). The results demonstrate the importance of

thermal management for small bodies exposed to *B*-fields in a solenoid coil. Temperature increases in mice from non-specific power absorption are minimised.

Results from heat transfer simulations described herein strongly suggest that single chamber continuous cooling is superior for regulating temperatures in small animals (radius ~1.9 cm). To the best of the authors' knowledge the only reported water cooling system for small animals is described by Jordan et al. [39] in which a mouse was sandwiched between two circulating water boluses, leaving significant portions of the mouse body exposed to air and thus not benefiting from cooling by circulating water. Such a discontinuous system can effectively cool regions in contact with the bolus, but cannot cool other regions. Thus portions of the animal body that are not in contact with the water and its efficient thermal transport are exposed to air relying on convective cooling. The latter is significantly less efficient and this disparity potentially creates a significant thermal gradient. The dual chamber discontinuous cooling simulations at 27°C described herein approximate the water cooling system reported by Jordan et al. [39].

A flow rate of 4L/min was chosen for the simulations to be consistent with the experimental conditions reported here. The flow rate used by Jordan et al. was not reported, and thus only approximate comparisons can be made. Temperatures predicted by simulations, however, are comparable to those reported in Jordan et al. [39] for both surface and core temperatures measured in mice, and they are directly comparable to the experimental results obtained in this study. It is worth noting that the mice were not anaesthetised in the referenced study [39] and the dual chamber water bolus was used to restrain mice during heating. Comparing the effects of anaesthesia within thermal modelling presents significant challenges. Low amplitude and low frequency AMF conditions are expected to deposit less heat into a body than the AMF parameters studied here. There is however, a recent increased interest in exploring hyperthermia with high frequency or high field AMF in order to maximise nanoparticle heating [34, 40, 41]. Given that eddy current heating of tissues is proportional to $(H \times f)^2$, it is expected that higher frequency/low amplitude combinations ought to have similar effects with lower frequency/high amplitude, assuming the product is comparable. Human clinical (whole-body or regional) applications of systems that produce fields exceeding the limit suggested by Atkinson et al. [20] (i.e. $f \times H < 4.85 \times 10^8$ A/m-s for a human torso having $r = 0.15$ m) is dubious; however, this limit may be exceeded for exposure of regions having smaller diameter, i.e. limbs or head. The latter has not been adequately explored, and thermal regulation as explored herein may have utility for such cases. An efficient system that regulates small animal temperatures to enable such experiments thus has potential utility.

Despite the advantages, it should be noted that the effectiveness of water cooling is limited to a shallow penetration depth. The maximum temperature in the simulated cylindrical domain was estimated in a range r~ 0.7–1.2 cm (Figure 5D). The limited penetration of the surface cooling effect should be considered when extending similar concept to a human torso, as the radius is ≈15 cm compared to 1.9 cm in the present simulations ($P_{non\text{-}specific} \propto r^2$). In addition, a coil generating inhomogeneous AMF was used. Exposure to such a field profile may generate a significantly lower SAR than would exposure to a homogeneous flux

density field that surrounds a greater percentage of the sample body, i.e. whole body. The latter case may be desired for systemic hyperthermia therapy.

Various methods have been proposed to reduce non-specific heating that arises from interactions of tissues with EM fields while maintaining a significant *B*-field intensity [7, 42] to achieve desired performance. Design and testing is generally limited to idealised models and modest power, typically 10–100 W. Such conditions may fail to reveal all challenges arising for clinical applications. For cancer therapy with nanoparticles, data from mouse models suggest that high power (>10 kW) may be required to realise therapeutic heating [30, 31] with currently available nanoparticle technology because nanoparticle formulations that produce therapeutic heat with low frequency, low amplitude AMF are not yet readily available [9]. For MNH, AC magnetic fields are used to activate the particles concentrated in cancer tissue. Non-specific heating of normal tissues can be limited by limiting both frequency and field intensity. Thus the frequency is typically limited to between 100 kHz and 300 kHz with intensities rarely exceeding 16 kA/m [6, 29]. For magnetite (Fe_3O_4)-based nanoparticles, such limited intensities fail to realise the full potential of hysteresis heating because the field amplitude is far below magnetisation saturation of magnetite (~85 kA/m, bulk value) [9]. Thus the technical challenge – how to extract sufficiently therapeutic heating from a small concentration of nanoparticles localised in target tissue –remains to be adequately addressed.

Encircling a sample or tissue with a continuous layer of cooling liquid that possesses suitable attributes to perform adequate and rapid cooling is thus desired. Depending upon the chosen AMF frequency, materials that possess additional beneficial properties, i.e. high dielectric, may be desired to enhance safety. Water is a unique substance possessing properties that interact with electromagnetic fields in complex ways, yielding an interesting frequency-dependent complex relative permittivity [43]. The effectiveness of water as a material for solenoid-based biomedical devices merits consideration in research with small animals.

The results obtained from both agar gel phantoms and mice with an AMF intensity of >80 kA/m and frequency 160 kHz generated by a four-turn solenoid coil are inconclusive for larger coils and bodies, and need further analysis for such systems. Agar gel phantoms can be made to have similar conductivity to that of muscle; therefore the initial temperature elevation data can be used to calculate net power deposited in the gels. While such an analysis is limited, the results can be helpful to design systems for further study, and to compare against simulated results. While the results reported here are intriguing, the small radius and thus low values of power absorption dictate caution for extrapolation to larger bodies exposed to fields in large-radius coils, or whole-body exposures. Additional effort to simulate both whole-body effects in small animals and regional exposure in larger radius samples are in progress.

Conclusions

In the present study we demonstrate an efficient way to thermally manage small animals during exposure to high amplitude AMF as often used in MNH, using a water jacket. The

water jacket has minimal or no interaction with the magnetic field, and does not attenuate the desired field intensity. The present thermal management model provides an effective way of performing more accurate and relevant thermal dosimetry and tumour growth delay studies in small animals because it reduces thermal gradients experienced by animal subjects during AMF exposure. Results from the water-based thermal management system for small animals are encouraging and should be explored for translation to larger systems to challenge its applicability in other model systems.

Acknowledgments

The authors wish to thank Valentin Nemkov and Robert Goldstein, both of AMF life Systems, for many informative and helpful discussions relating to AMF devices, and to Thomas Budinger for many helpful discussions related to electromagnetic fields and interactions with tissues.

References

1. Ehrmann K, Saillen N, Vincent F, Stettler M, Jordan M, Wurm FM, et al. Microfabricated solenoids and Helmholtz coils for NMR spectroscopy of mammalian cells. Lab Chip. 2007; 7:373–380. [PubMed: 17330169]
2. Minard KR, Wind RA. Solenoidal microcoil design – Part I: Optimizing RF homogeneity and coil dimensions. Concepts Magn Reson. 2000; 13:128–142.
3. McCann C, Sherar MD. Development of a novel loosely wound helical coil for interstitial radiofrequency thermal therapy. Phys Med Biol. 2006; 51:3835–3850. [PubMed: 16861784]
4. Ellinger DC, Chute FS, Vermeulen FE. Evaluation of a semi-cylindrical solenoid as an applicator for radio-frequency hyperthermia. IEEE Trans Biomed Eng. 1989; 36:987–994. [PubMed: 2793199]
5. Tasci TO, Vargel I, Arat A, Guzel E, Korkusuz P, Atalar E. Focused RF hyperthermia using magnetic fluids. Med Phys. 2009; 36:1906–1912. [PubMed: 19544810]
6. Jordan, A.; Wust, P.; Scholz, R.; Faehling, H.; Krause, J.; Felix, R. Magnetic fluid hyperthermia (MFH). In: Hafeli, U.; Zborowski, M.; Schutt, W., editors. Scientific and Clinical Applications of Magnetic Carriers. New York: Plenum Press; 1997. p. 569-595.
7. Stauffer PR, Sneed PK, Hashemi H, Phillips TL. Practical induction heating coil designs for clinical hyperthermia with ferromagnetic implants. IEEE Trans Biomed Eng. 1994; 41:17–28. [PubMed: 8200664]
8. Rosensweig RE. Heating magnetic fluid with alternating magnetic field. J Magn Magn Mat. 2002; 252:370–374.
9. Bordelon D, Cornejo C, Gruettner C, DeWeese TL, Ivkov R. Magnetic nanoparticle heating efficiency reveals magneto-structural differences when characterized with a wide ranging and high amplitude alternating magnetic field. J Appl Phys. 2011; 109:124904.
10. Kashevsky BE, Kashevsky SB, Prokhorov IV. Dynamic magnetic hysteresis in a liquid suspension of acicular maghemite particles. Particuology. 2009; 7:451–458.
11. Ellinger DC, Vermeulen FE. Evaluation of a semi-cylindrical solenoid as an applicator for radio-frequency hyperthermia. IEEE Trans Biomed Eng. 1989; 36:987–994. [PubMed: 2793199]
12. Lin, JC.; Bernardi, P. Computational methods for predicting field intensity and temperature change. In: Barnes, FS.; Greenebaum, B., editors. Bioengineering and biophysical aspects of electromagnetic fields. 3. Boca Raton: CRC Press; 2007. p. 293-380.
13. Liu F, Zhao H, Crozier S. On the induced electric field gradients in the human body for magnetic stimulation by gradient coils in MRI. IEEE Trans Biomed Eng. 2003; 50:804–815. [PubMed: 12848348]
14. Wang Q, Deng ZS, Liu J. Theoretical evaluations of magnetic nanoparticle-enhanced heating on tumor embedded with large blood vessels during hyperthermia. J Nanopart Res. 2012; 14:974–984.

15. Szasz, A.; Szasz, O.; Szasz, N. Physical background and technical realizations of hyperthermia. In: Baronzio, GF.; Hager, ED., editors. Hyperthermia in Cancer Treatment: A primer. New York: Landes Bioscience and Springer; 2006. p. 27-52.
16. Adair ER, Black DR. Thermoregulatory responses to RF energy absorption. Bioelectromagnetics. 2003; 6:S17–38. [PubMed: 14628305]
17. Black, DR. Thermoregulation in the presence of radio frequency fields. In: Barnes, FS.; Greenebaum, B., editors. Biological and Medical Aspects of Electromagnetic Fields. 3. Boca Raton, FL: CRC Press; 2006. p. 215-226.
18. Cerchiari, U. Hyperthermia, physics, vector potential, electromagnetic heating: A primer. In: Baronzio, GF.; Hager, ED., editors. Hyperthermia in Cancer Treatment: A primer. New York: Landes Bioscience and Springer; 2006. p. 3-18.
19. Polk, C. Introduction. In: Barnes, FS.; Greenebaum, B., editors. Biological and Medical Aspects of Electromagnetic Fields. 3. Boca Raton, FL: CRC Press; 2006. p. xiii-xxvi.
20. Atkinson WJ, Brezovich IA, Chakraborty DP. Usable frequencies in hyperthermia with thermal seeds. IEEE Trans Biomed Eng. 1984; 31:70–75. [PubMed: 6724612]
21. Brezovich, IA. Low frequency hyperthermia: Capacitive and ferromagnetic thermoseed methods. In: Paliwal, B.; Hetzel, FW.; Dewhirst, MW., editors. Biological, Physical, and Clinical Aspects of Hyperthermia. Ann Arbor, MI: American Institute of Physics; 1988. p. 82-111.Medical Physics Monograph 16
22. Dewhirst, MW.; Jones, E.; Samulski, T.; Vujaskovic, Z.; Li, C.; Prosnitz, L. Hyperthermia. In: Kufe, DW.; Pollock, RE.; Weichselbaum, RE.; Bast, RC.; Gansler, TS., editors. Cancer Medicine. 6. Hamilton, Ontario: BC Decker; 2003. p. 623-636.
23. Dewhirst MW, Viglianti BL, Lora-Michiels M, Hanson M, Hoopes PJ. Basic principles of thermal dosimetry and thermal thresholds for tissue damage from hyperthermia. Int J Hyperthermia. 2003; 19:267–294. [PubMed: 12745972]
24. Roti Roti JL. Heat-induced alterations of nuclear protein associations and their effects on DNA repair and replication. Int J Hyperthermia. 2002; 23:3–15. [PubMed: 17575719]
25. Horsman MR, Overgarrd J. Hyperthermia: A potent enhancer of radiotherapy. Clin Oncol. 2007; 19:418–426.
26. Hunt CR, Pandita RK, Laszlo A, Higashikubo R, Agarwal M, Kitamura T, et al. Hyperthermia activates a subset of ataxia-telangiectasia mutated effectors independent of DNA strand breaks and heat shock protein 70 status. Cancer Res. 2007; 67:3010–3017. [PubMed: 17409407]
27. van der Zee J. Heating the patient: A promising approach? Ann Oncol. 2002; 13:1173–1184. [PubMed: 12181239]
28. Candeo A, Dughiero F. Numerical FEM models for the planning of magnetic induction hyperthermia treatments with nanoparticles. IEEE Trans Magn. 2009; 45:1658–1661.
29. Wust P, Gneveckow U, Johannsen M, Böhmer D, Henkel T, Kahmann F, et al. Magnetic nanoparticles for interstitial thermotherapy – Feasibility, tolerance and achieved temperatures. Int J Hyperthermia. 2006; 22:673–685. [PubMed: 17390997]
30. DeNardo SJ, DeNardo GL, Natarajan A, Miers LA, Foreman AR, Gruettner C, et al. Thermal dosimetry predictive of efficacy of ^{111}In-ChL6 nanoparticle AMF-induced thermoablative therapy for human breast cancer in mice. J Nuc Med. 2007; 48:437–444.
31. Dennis CL, Jackson AJ, Borchers JA, Hoopes PJ, Strawbridge R, Foreman AR, et al. Nearly complete regression of tumors via collective behavior of magnetic nanoparticles in hyperthermia. Nanotechnology. 2009; 20:395103. [PubMed: 19726837]
32. Trakic A, Liu F, Crozier S. Transient temperature rise in a mouse due to low-frequency regional hyperthermia. Phys Med Biol. 2006; 51:1673–1691. [PubMed: 16552097]
33. Ivkov R, DeNardo SJ, Daum W, Foreman AR, Goldstein RC, Nemkov VS, DeNardo GL. Application of high amplitude alternating magnetic fields for heat induction of nanoparticles localized in cancer. Clin Cancer Res. 2005; 11:S7093–7103.
34. Bordelon D, Goldstein R, Nemkov V, Kumar A, Jackowski J, DeWeese TL, Ivkov R. Modified solenoid coil that efficiently produces high amplitude AC magnetic fields with enhanced uniformity for biomedical applications. IEEE Trans Magn. 2012; 48:47–52.

35. Ulrich J. Comparison of different techniques for the treatment of lossy dielectric/magnetic bodies within the method of moments formulations. AEU Int J Electron Commun. 2000; 54:163–173.

36. Harrington, RF. Field Computation by Moment Methods. New York: IEEE Press; 1993.

37. Grover, FW. Inductance Calculations. New York: Dover; 1973.

38. Solazzo SA, Liu Z, Lobo SM, Ahmed M, Hines-Peralta AU, Lenkinski RE, et al. Radiofrequency ablation: Importance of background tissue electrical conductivity – An agar phantom and computer modeling study. Radiology. 2005; 236:495–502. [PubMed: 16040906]

39. Jordan A, Scholz R, Wust P, Fähling H, Krause J, Wlodarczyk W, et al. Effects of magnetic fluid hyperthermia (MFH) on C3H mammary carcinoma in vivo. Int J Hyperthermia. 1997; 13:587–605. [PubMed: 9421741]

40. Dutz S, Kettering M, Hilger I, Müller R, Zeisberger M. Magnetic multicore nanoparticles for hyperthermia -Influence of particle immobilization in tumour tissue on magnetic properties. Nanotechnology. 2011; 22:265102. [PubMed: 21576784]

41. Fortin JP, Gazeau F, Wilhelm C. Intracellular heating of living cells through Néel relaxation of magnetic nanoparticles. Eur Biophys J. 2008; 37:223–228. [PubMed: 17641885]

42. Park B, Neuberger T, Webb AG, Bigler DC, Collins CM. Faraday shields within a solenoidal coil to reduce sample heating: Numerical comparison of designs and experimental verification. J Magn Reson. 2010; 202:72–77. [PubMed: 19879784]

43. Kaatze U. Complex permittivity of water as a function of frequency and temperature. J Chem Eng Data. 1989; 34:371–374.

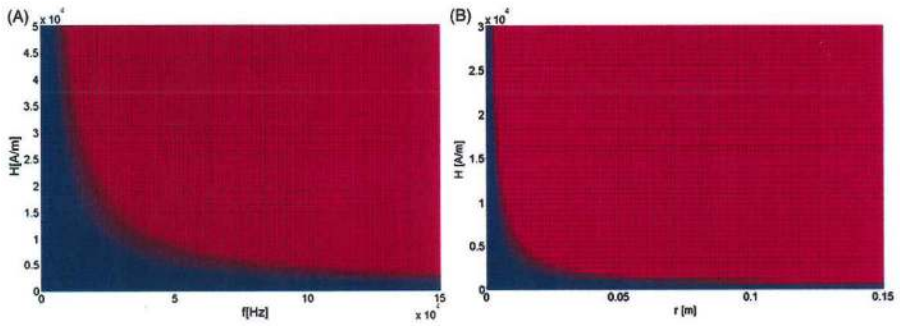

Figure 1.

Calculated allowable power deposition for a simulated cylinder of muscle tissue based on limits proposed by Atkinson et al. [25], with (A) varying frequency (*f*) and field amplitude (*H*) for cylinder having a radius, *r*= 0.15 m, and (B) varying field amplitude (*H*) and radius (*r*) of simulated tissue at a fixed frequency of 160 kHz. Blue zones display combinations that do not exceed maximum allowable limits, whereas red zones represent fields and exposures that exceed tolerance limits.

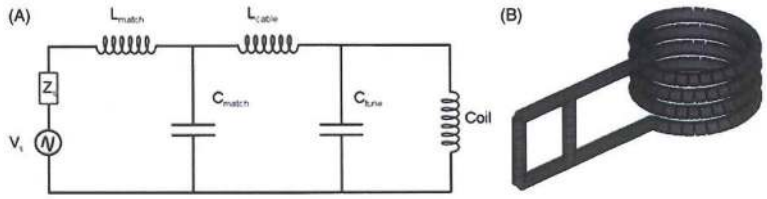

Figure 2.

(A) Circuit diagram of the AMF system. (B) The four turn solenoid coil modelled using MoM. The coil inner diameter is 45 mm and coil length is 32 mm.

Figure 3.
Picture of the 4-turn solenoid coil, water jacket and mouse chamber with anaesthetised mouse inside.

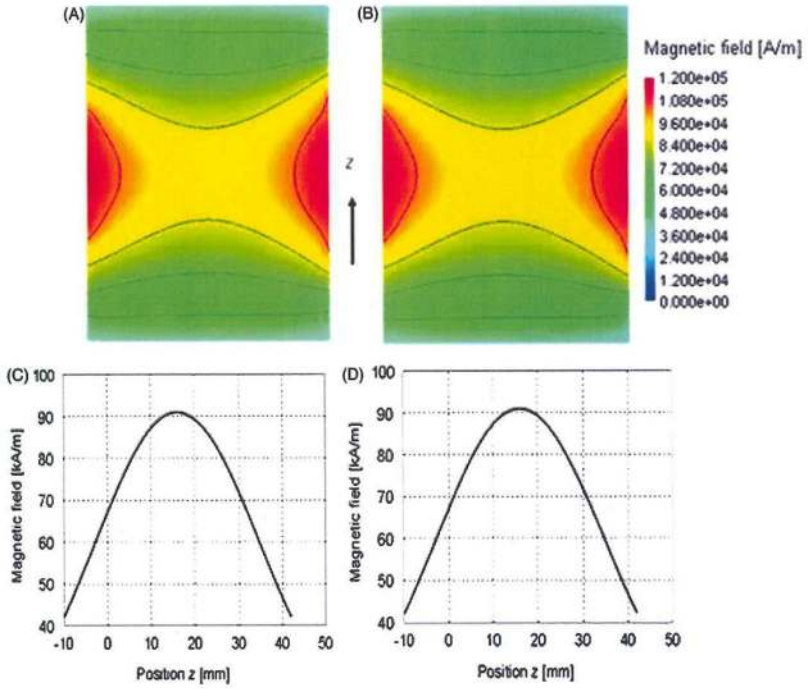

Figure 4.

Magnetic field across the (x–z plane) in the coil in the sample volume with no water (A) and with water (B) in the jacket; Magnetic field profile along the middle of solenoid in z direction without water (C) and with water (D) for 8 kW (peak) input power to AMF coil.

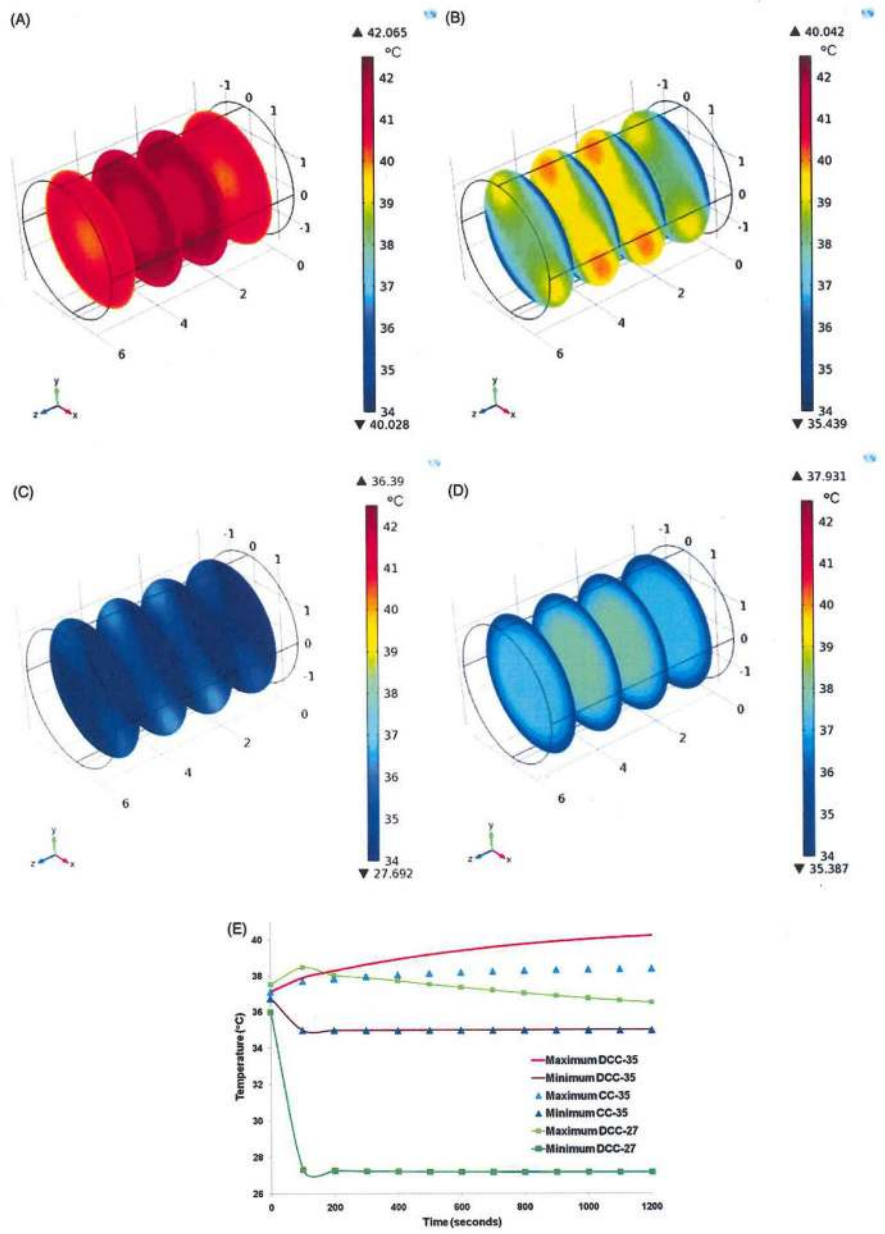

Figure 5.

Temperature profile at the end of 1200 s of AMF exposure. (A) No external cooling. (B) Dual chamber discontinuous cooling at 35°C. (C) Dual chamber discontinuous cooling at 27°C. (D) Single chamber continuous cooling at 35°C. (E) Comparison of maximum and minimum temperatures in the domain among cases B, C and D.

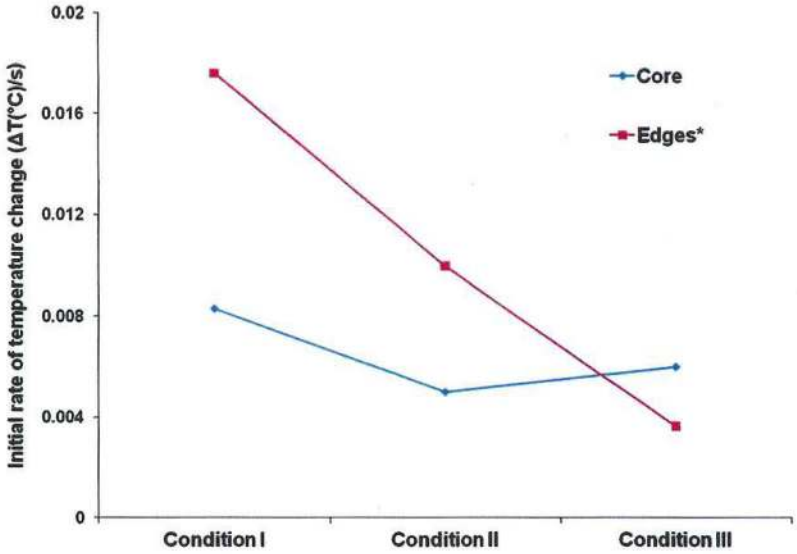

Figure 6.
Comparison of net initial rate of temperature change in the gels for conditions I, II, and III.

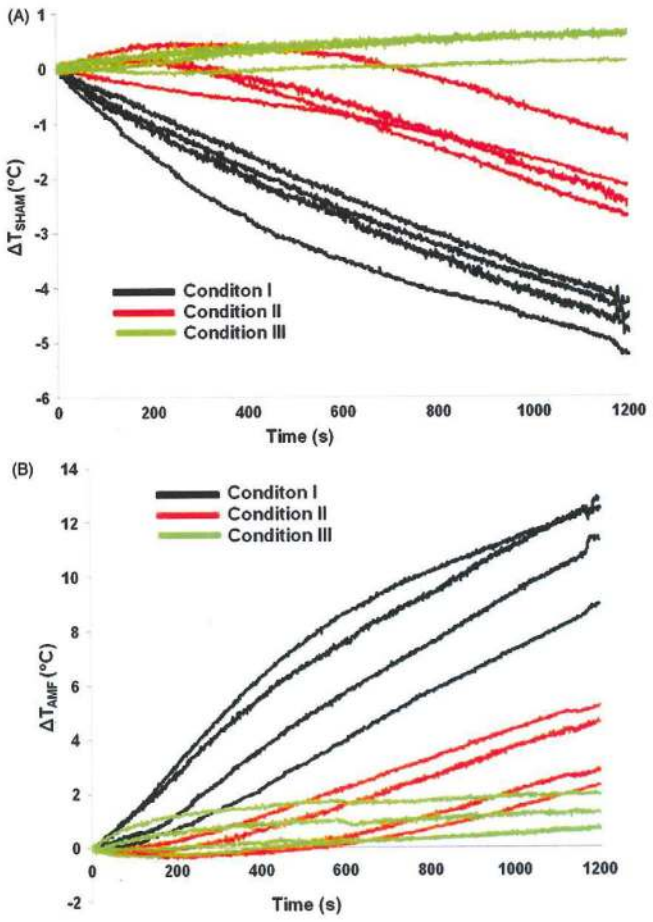

Figure 7.

Observed temporal change in temperatures of (A) individual mice at each of the three conditions (I, II, and III) with no AMF, and (B) with 20 min exposures to AMF having amplitude of 84 kA/m. Displayed are corrected ($T(t) - T(0)$) data obtained from each of four temperature probes (two placed s.c. in left and right thorax, one affixed to skin surface of abdomen, and one inserted into rectum.

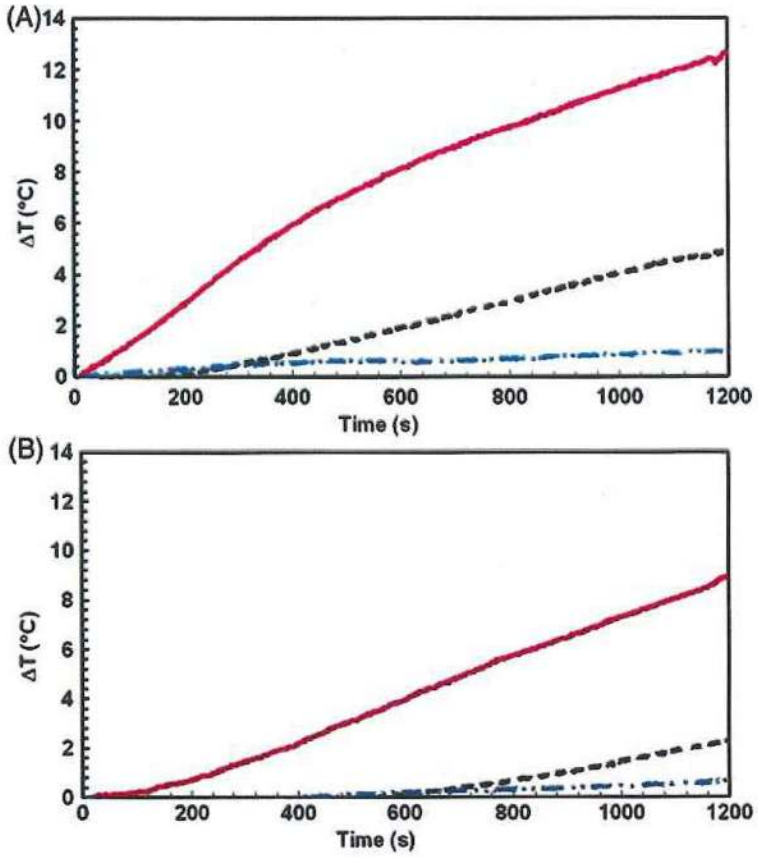

Figure 8.

Corrected temperature change as measured in the thorax (A) and rectum (B) for mouse exposed to AMF with no water, i.e. condition I (solid line), mouse exposed to AMF with water but no active cooling, i.e. condition II (dashed line), and mouse exposed to AMF with actively cooled water, i.e. condition III (dash-dot-dot). Subcutaneous thoracic temperatures were averaged for both left and right side. In all cases the temperature change for each temperature probe was calculated from measured temperatures and the total change of temperature was estimated after subtracting temperature changes obtained from sham controls.

Table I

Physical parameters and data used for thermal simulations.

Parameter	Symbol	Value
Thermal conductivity	k_t	0.5 W/(m.K)
Density of tissue	ρ_τ	1080 kg/m^3
Specific heat of tissue	C_{t_p}	3680 J/(kg.K)
Blood perfusion constants	$\omega\rho_b C_{bp}$	1065 W/(m^3°C)
Arterial temperature	T_b	37°C

Table II

AMF coil electrical properties.

Analytical		Numerical		Experimental	
Inductance	**Resistance**	**Inductance**	**Resistance**	**Inductance**	**Resistance**
740 nH	5.4 mΩ	738 nH	4.6 mΩ	753 nH	5.97 mΩ

Table III

AMF coil voltage, V and magnetic field, kA/m.

	Magnetic field (kA/m)		
Voltage (peak)	**Analytical**	**Numerical**	**Experimental**
137	16.3	17.3	15.2
275	32.8	35.2	33.7
410	49.0	52.2	51.9
535	63.8	68.3	69.0
690	82.4	87.4	86.7

Table IV

Comparison of experimentally measured magnetic field (kA/m) with and without water jacket.

No water jacket		Water jacket		
Set voltage	**Magnetic field**	**Set voltage**	**Magnetic field**	**% Change**
81	16.03	80	15.99	0.24
270	39.76	270	38.46	3.27
457	62.12	455	57.35	7.67
631	80.74	628	76.48	5.27

Table V

Gel phantom temperature data.

	Corrected ΔT (°C)†	
Exposure	**Core (0 mm)**	**Edge★**
Condition 1: AMF	18.7	20.5
Condition 2: AMF	11.2	11.5
Condition 3: AMF	2.4	1.1

†Values reported are the difference at each time step (1-s intervals) with initial temperature ($t = 0$ s), i.e. $\Delta T = T(t) - T(t = 0)$. No sham data were taken.

★Reported value represents a mean taken from two temperature probes inserted into the gel at the wall of the vessel in contralateral positions.

Table VI

Mouse temperature data.

Mouse no.	Exposure★	Mass (kg)	Initial temperature (°C)				Final temperature (°C) ($\Delta T = T_{final} - T_{initial}$)†			
			LT★★	RT★★	Re★★	B★★	LT★★	RT★★	Re★★	B★★
1	Condition III: Sham	0.021	33.7	34.8	33.7	34.6	34.4 (0.7)	35.4 (0.6)	33.9 (0.2)	35.2 (0.6)
2	Condition III: AMF	0.026	35.5	36.6	36.2	36.2	36.9 (1.4)	38.6 (2.0)	37.0 (0.8)	38.7 (2.5)
3	Condition II-Sham	0.021	33.5	34.7	33.2	33.8	30.9 (−2.6)	32.3 (−2.4)	31.1 (−2.1)	32.5 (−1.3)
4	Condition II-AMF	0.021	35.6	36.6	35.4	36.4	38.2 (2.6)	38.9 (2.3)	35.7 (0.3)	38.0 (1.6)
5	Condition I-AMF	0.021	31.9	33.6	33.7	33.6	40.1 (8.2)	41.8 (8.2)	37.6 (3.9)	40.4 (6.8)
6	Condition I-Sham	0.021	33.8	35.1	34.6	34.9	29.6 (−4.2)	30.4 (−4.7)	29.4 (−5.2)	30.4 (−4.5)

†Values in parentheses are the difference of initial and final temperatures for corresponding probes.

★Condition I, no water; Condition II, water in jacket; Condition III, water with active cooling maintained at 35°C. AMF exposure was 20 min at amplitude 86 kA/m and frequency 160 kHz.

★★Placement of the fibre-optic temperature probes: LT, subcutaneous left thorax; RT, subcutaneous right thorax; Re, rectum; B, skin of abdomen.